

Image States and Excitons at Insulator Surfaces with Negative Electron Affinity

Michael Rohlfing,¹ Neng-Ping Wang,² Peter Krüger,² and Johannes Pollmann²

¹*School of Engineering and Science, International University Bremen, P.O. Box 750561, 28725 Bremen, Germany*

²*Institut für Festkörpertheorie, Universität Münster, 48149 Münster, Germany*

(Received 7 August 2003; published 19 December 2003)

We discuss electronic excitation processes at two ionic insulator surfaces, LiF(001)-(1 × 1) and MgO(001)-(1 × 1), within *ab initio* many-body perturbation theory. Because of the negative electron affinity of the surfaces, the lowest unoccupied electronic states are image states located in the vacuum outside the surface. Excitations of electrons from the surface layer into these image states are much lower in energy than the bulk excitons. They are responsible for characteristic surface features in the electron energy-loss spectra of LiF(001) and MgO(001).

DOI: 10.1103/PhysRevLett.91.256802

PACS numbers: 73.20.At, 73.20.Mf, 79.20.Uv

Surface-sensitive spectra of wide-gap insulators often exhibit signatures of surface excitons several eV below the bulk excitations [1–4]. It has already been suggested in Ref. [2] that surface excitations at such low-energy may be related to image states if the surface has negative electron affinity (NEA) [5]. At such surfaces the conduction-band minimum (CBM) is higher in energy than the vacuum level (E_{vac}). As a result, the image states of the vacuum, having energies below E_{vac} , are located in the fundamental band gap of the insulator. Image states, that result from the electrostatic interaction between an electron outside the surface and the polarizability in the material [6], are usually in energetic resonance with substrate states [apart from systems such as, e.g., Cu(100) where they lie in band pockets] and are thus not easily detectable. At NEA insulator surfaces, however, they constitute the onset of unoccupied electronic states. Surface excitons between occupied substrate states and the image states are thus much lower in energy than the substrate bulk excitons and lead to predominant features in, e.g., electron-energy loss spectroscopy (EELS) [1–3].

The concept of surface excitons involving the image states is hard to prove for several reasons. First, the surface peaks in the EELS spectra provide only indirect indications to the image states and do not allow for a quantitative analysis. Direct excitation of the image states, as in inverse photoemission spectroscopy, is very difficult due to charging effects on insulator surfaces [5]. Second, surface excitons are strongly affected by electronic many-body effects and electron-hole interaction, i.e., the peak position in the EELS spectra cannot be interpreted as the energy level of the image state. In addition, image states form a bridge between localized and delocalized electronic states. The influence of electronic correlation thus differs from the many-body effects on bulk states and is much more difficult to address in a theoretical approach. A quantitative analysis of the image states and the corresponding excitations is thus still lacking, both in theory and experiment.

Here we investigate the image states and their excitations within *ab initio* many-body perturbation

theory (MBPT) designed for excited electronic states [7,8]. Starting from the electronic ground state within the local-density approximation (LDA), exchange-correlation effects are described by the electron self-energy operator and the corresponding electron-hole interaction, which we evaluate within the *GW* approximation. This approach yields highly accurate quasiparticle (QP) excitations (i.e., electrons and holes) and coupled electron-hole excitations. The latter result from the equation of motion (Bethe-Salpeter equation, BSE) of the two-particle Green function. From the electron-hole states the macroscopic dielectric function is evaluated and optical as well as EELS spectra are analyzed.

The surface is represented by slabs of five or six atomic layers in a supercell configuration (up to 45 Å in height). We use atom-centered Gaussian orbitals [8] to expand the wave functions, self-energy operator, and electron-hole interaction. In addition, slowly decaying *s*-type orbitals (decay constants 0.14 a.u.) are placed in the vacuum region above one surface (at the "virtual" atomic positions, up to 25 Å in height) to represent the vacuum states.

Most of the following discussion focuses on the LiF(001)-(1 × 1) surface at which the addressed effects are most pronounced. Results for MgO(001)-(1 × 1) are included for further reference. Figure 1 shows the QP band structure of the LiF(001)-(1 × 1) surface. The most relevant excitation energies are summarized in Table I. The vacuum level is located 11.6 eV above E_{VBM} and 2.8 eV below E_{CBM} , i.e., the ionization potential amounts to 11.6 eV and LiF(001) has negative electron affinity, therefore.

The bands of the supercell can be classified in three groups. (i) Below E_{VBM} the F 2*p* valence states are found. (ii) At $E_{\text{CBM}} = E_{\text{vac}} + 2.8$ eV we find the onset of the LiF conduction bands. They hybridize with higher vacuum states, i.e., the labeling as LiF bands is not strictly correct. (iii) Between the vacuum level and the onset of the projected conduction bands several vacuum states occur. They form a discrete set of bands rather than a continuous spectrum due to the finite thickness (25 Å) of the vacuum layer filled with basis orbitals, in which the vacuum states

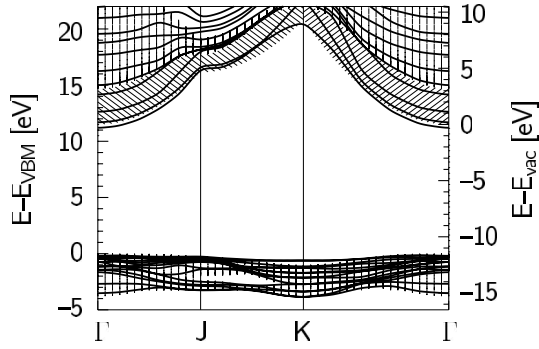


FIG. 1. Quasiparticle band structure of the LiF(001)-(1 × 1) surface, calculated within the *GW* approximation. The left-hand energy scale refers to the LiF valence-band maximum (VBM) while the right-hand energy scale refers to the vacuum level. The vertically shaded areas below E_{VBM} and above $E_{\text{VBM}} + 14.4$ eV indicate the projected LiF bulk band structure. The shaded area below the LiF bulk CBM (shaded in a left- or right-slanted manner for better visibility) indicates the range of vacuum states, starting at $E_{\text{vac}} + (\hbar\mathbf{k})^2/2m$ with \mathbf{k} being the two-dimensional wave vector parallel to the surface.

can exist. Throughout the whole surface Brillouin zone there is an energy range of about 3 eV width between the lower limit of projected vacuum states and the lower limit of LiF conduction states. In this range the vacuum states cannot mix with LiF states and are forced to reside outside the material. Nevertheless, the vacuum states are significantly influenced by the potential of the LiF surface, which is displayed in Fig. 2(a). At $z < 0$ the potential shows the oscillations of bulk LiF. At $z > 0$ the potential is still attractive, leading to the occurrence of a slightly bound image state at energy $E_{\text{vac}} - 0.3$ eV (for $\mathbf{k} = 0$).

The QP states result from the Dyson equation [7], including the self-energy operator Σ which describes the electronic many-body effects in a more reliable way

TABLE I. Excitation energies of the LiF(001)-(1 × 1) and MgO(001)-(1 × 1) surface calculated within many-body perturbation theory, in comparison with experiment. All band-structure energies refer to the valence-band maximum.

[eV]	LiF(001)		MgO(001)	
	Theory	Expt.	Theory	Expt.
Bulk gap	14.4	14.2 ^a	7.8	7.83 ^d
Bulk exciton	12.7	12.59 ^a	7.7	7.69 ^d
Ionization potential	11.6	11.8 ^b	7.4	
Image state (at Γ)	11.3		6.9	
Singlet exciton	9.3		5.9	
EELS peak	9.9	10.5 ^c	~6.5	6.3 ^e
Triplet exciton	9.2		5.8	

^aRef. [9]

^bRef. [5]

^cRef. [3]

^dRef. [10]

^eRef. [4]

than the DFT-LDA exchange-correlation potential V_{xc} . In the present case the matrix of the self-energy correction operator, $\langle \psi_{m\mathbf{k}}^{\text{LDA}} | (\Sigma - V_{\text{xc}}) | \psi_{m'\mathbf{k}}^{\text{LDA}} \rangle$, is not diagonal in the LDA states, in particular, in those states located in the vacuum. Therefore, the LDA states do not represent the true QP states and perturbative treatment of $(\Sigma - V_{\text{xc}})$ is not sufficient. Instead, full diagonalization of the QP Hamiltonian is required. The most dramatic effect of this procedure is observed for the image state [see Fig. 2(c)]. Its LDA wave function is localized within about 4 Å of the surface, whereas its QP wave function is much more delocalized and extends up to 20 Å into vacuum. Simultaneously, its band-structure energy is raised from $E_{\text{vac}} - 0.9$ eV in LDA to $E_{\text{vac}} - 0.3$ eV in the QP spectrum. We note that simple first-order perturbation treatment of $(\Sigma - V_{\text{xc}})$ leaves the wave function of the image state unchanged and raises its energy to $E_{\text{vac}} + 0.4$ eV. Similar effects have been observed for unoccupied states in molecules [11], for image states on metals [12], and for semiconductor dangling-bond surface states in resonance with bulk states [13].

The reason for the delocalization when going from LDA to *GW* becomes clear in Fig. 2(b) which shows the self-energy contribution to the potential of panel a. In order to visualize the nonlocal self-energy and to compare it with the local LDA $V_{\text{xc}}(\mathbf{r})$, we map Σ onto a local potential $V_{\text{loc}}(\mathbf{r})$, following a suggestion of White *et al.* [12]: $V_{\text{loc}}(\mathbf{r}) := \sum_m \langle \mathbf{r} | \psi_{m\mathbf{k}}^{\text{LDA}} \rangle \langle \psi_{m\mathbf{k}}^{\text{LDA}} | \Sigma | \psi_{\text{image},\mathbf{k}}^{\text{QP}} \rangle \langle \mathbf{r} | \psi_{\text{image},\mathbf{k}}^{\text{QP}} \rangle$ where $|\psi_{\text{image},\mathbf{k}}^{\text{QP}}\rangle$ is the image state in question ($\mathbf{k} = 0$)

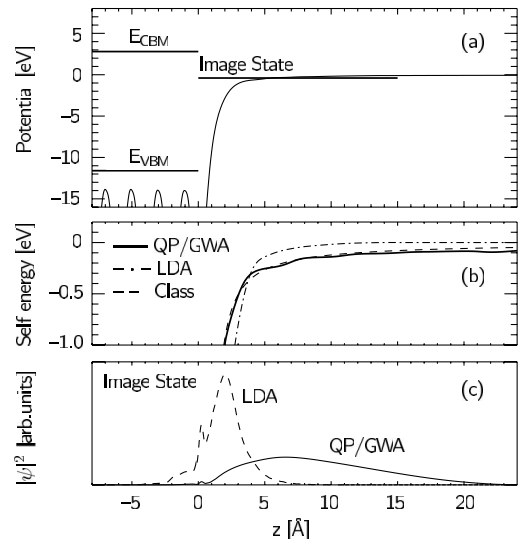


FIG. 2. Panel (a): *xy*-averaged single-particle potential at the LiF(001)-(1 × 1) surface along the surface normal, with respect to the vacuum level (= 0 eV). The surface atomic layer is located at $z = 0$. The horizontal lines indicate the QP energies of the bulk VBM and CBM and of the image state (at $\mathbf{k} = 0$). Panel (b): *xy*-averaged self-energy of the image state (see text). Panel (c): *xy*-averaged charge density of the image-state wave function (at $\mathbf{k} = 0$) along the surface normal. The solid (dashed) line refers to the QP (LDA) wave function.

in Fig. 2). By construction, $V_{\text{loc}}(\mathbf{r}) \cdot \langle \mathbf{r} | \psi_{\text{image}, \mathbf{k}}^{QP} \rangle = \langle \mathbf{r} | \Sigma | \psi_{\text{image}, \mathbf{k}}^{QP} \rangle$, i.e., V_{loc} reproduces the action of Σ on $|\psi_{\text{image}, \mathbf{k}}^{QP}\rangle$ and may thus be interpreted as a “local” self-energy, seen by $|\psi_{\text{image}, \mathbf{k}}^{QP}\rangle$. This local self-energy is displayed in Fig. 2(b) (after averaging over x and y). It nicely agrees with a classical image potential $V_{\text{im}}(z) = -1/4 \cdot (\epsilon - 1)/(\epsilon + 1) \cdot e^2/(z - z_0)$ [6] [dashed line in Fig. 2(b)] with $\epsilon = 1.9$ being the LiF bulk dielectric constant and z_0 the position of the image plane (choosing $z_0 = 0.8 \text{ \AA}$ yields the best agreement with the calculated self-energy) [14]. Such an image potential, which is a common concept for discussing image states on metal surfaces, originates from the electrostatic interaction of the electron (outside the surface) with polarization charges inside the substrate. This interaction constitutes the leading term of the GW self-energy at large distance.

The LDA V_{xc} potential and the (local) GW self-energy show very different behavior. Within LDA V_{xc} goes to zero exponentially in the vacuum, giving rise to the localization of the LDA image state [see Fig. 2(c)]. The GW self-energy, on the other hand, decays much more slowly. We find that $\Sigma^{GW} > V_{\text{xc}}$ for $z < 4 \text{ \AA}$ and $\Sigma^{GW} < V_{\text{xc}}$ for $z > 4 \text{ \AA}$, which causes the delocalization of the QP wave function when going from LDA to GW . The maximum of the wave function is now at $z = 6.5 \text{ \AA}$, in good agreement with the value of $z_0 + 4(\epsilon + 1)/(\epsilon - 1) \cdot a_{\text{bohr}} = 7.6 \text{ \AA}$ which would result from the classical image potential. Our calculated QP energy of -0.3 eV is somewhat lower than the ground-state energy in the image potential of $-1/16[(\epsilon - 1)/(\epsilon + 1)]^2 \text{ Ry} = -0.08 \text{ eV}$. The difference, which is commonly attributed to a “quantum defect,” is due to the slight amplitude of the image state in the surface atom layer and to the modification of the potential due to the atomic structure of the surface.

On MgO(001)-(1 × 1) similar effects are observed (see Table I). MgO(001) has an ionization potential of 7.4 eV and a NEA of 0.4 eV, only, which is much smaller than for LiF(001). The image state is thus less strongly repelled from the material. Its energy amounts to $E_{\text{vac}} - 1.2 \text{ eV}$ in LDA and $E_{\text{vac}} - 0.5 \text{ eV}$ in the GW approximation. Different from LiF, its LDA wave function is qualitatively correct, i.e., the off-diagonal matrix elements of $(\Sigma - V_{\text{xc}})$ are small and the wave function does not change significantly from LDA to GW .

Experimental information about the surface states is available from electron-hole excitations. We therefore solve the Bethe-Salpeter equation of coupled electron-hole states and evaluate the dielectric function of the slab. Together with that of the bulk, it allows us to discuss optical spectra and EELS spectra. The surface excitons depend on their two-dimensional total momentum \mathbf{Q} . We first focus on $\mathbf{Q} = 0$ and analyze the resulting exciton states. For the discussion of the EELS spectrum, we consider the \mathbf{Q} dependence of the dielectric function.

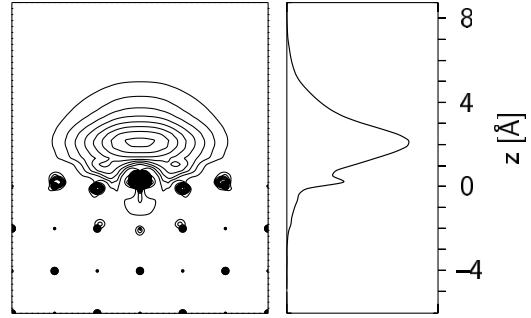


FIG. 3. Lowest singlet exciton state of the LiF(001)-(1 × 1) surface: Two-dimensional projection (side view) of the probability density, showing the distribution of the excited electron (relative to the hole at the surface F atom in the center of the plot). Small (large) dots denote Li (F) atoms. The line plot on the right-hand side shows the xy averaged probability distribution of the electron.

From the band structure it is clear that the lowest electron-hole excitations occur between the upper valence states and the low-lying vacuum states. These transitions can be excited as singlet-to-singlet or as singlet-to-triplet transitions. We find a large number of such states, starting at an excitation energy of 9.3 eV for the singlet and 9.2 eV for the triplet exciton. These energies are much lower than the transition energy of 12.7 eV for the bulk excitons. They are also much lower than the transition energy of 12.3 eV between the surface-modified valence and conduction states of bulk LiF that we discussed in an earlier study [8]. The binding energy of the surface exciton is slightly larger (2.0 eV for the singlet) than for the bulk exciton (1.7 eV). We attribute this increase to the weaker dielectric screening outside the surface.

More insight into the exciton state can be gained from its two-particle wave function. Figure 3 shows the distribution of the excited electron, relative to the hole at the surface F atom in the center of the plot. The line plot on the right-hand side shows the z dependence of the same quantity after averaging over x and y . We note in passing that the hole mainly consists of F $2p_{x/y}$ orbitals in the surface layer [8]. The electron is mostly located in the vacuum region, but has a contribution on the surface atom layer as well. Note that the electron is much more strongly localized than the QP wave function of the image state. The delocalization of the image states, as resulting from the self-energy operator, is overruled by the attraction of the electron to the hole in the surface layer. The excited electron is not just composed from the image state but from several other QP states as well, including contributions from the LiF conduction states, as controlled by the electron-hole interaction.

We note in passing that when the BSE is solved in the basis of the LDA states instead of the QP states [i.e., when the off-diagonal matrix elements of $(\Sigma - V_{\text{xc}})$ are neglected], the resulting excitations are only slightly

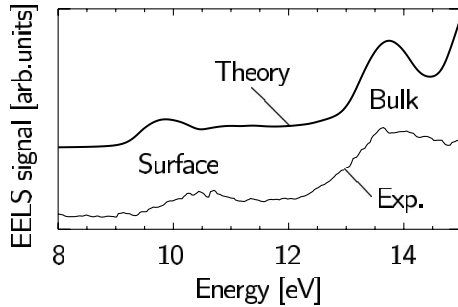


FIG. 4. Calculated EELS spectrum (upper curve) in comparison with experimental data (lower curve) by Mabuchi [3]. Electron impact energy and angle are 200 eV and 45°. The calculated data include Lorentzian broadening of 0.5 eV to ease the comparison with the measured data.

different. The excitation energies of the singlet and triplet exciton are lowered by 0.3 eV, and the charge distribution of the excited electron is slightly more localized than shown in Fig. 3. Apparently, the details of the self-energy operator (like its off-diagonal matrix elements) are essential for the single-particle excitations, but are less important for two-particle excitations that are dominated by the electron-hole interaction.

For comparison with experiment, we evaluate the EELS spectrum which is mainly given by $\text{Im}[-1/(1 + \epsilon(\omega))]$, with $\epsilon(\omega)$ being the macroscopic dielectric constant [15]. We include the influence of the bulk, as well as of momentum transfer, electron impact energy, and impact angle [15]. A characteristic example of such a spectrum is shown in Fig. 4 together with measured data from Ref. [3]. The present situation can be analyzed in terms of a thin layer with a surface dielectric function on top of a semi-infinite substrate [16]. Consequently, both surface and bulk states occur in the spectrum with a characteristic amplitude ratio. The bulk peak occurs about 1 eV above the bulk exciton energy of 12.7 eV since the EELS spectrum becomes maximal for energies at which $\epsilon(\omega) = -1$, which is above the exciton resonance. At 9.9 eV (10.5 eV in experiment) a surface peak is observed. This peak is higher in energy than the lowest singlet surface exciton (9.3 eV) for two reasons. First, the sensitivity of EELS to features in $\text{Im}[-1/(1 + \epsilon(\omega))]$ induces a blueshift similar to (but not as strong as) the bulk peak. Second, EELS includes momentum transfer, so it is sensitive to excitons not only at the Γ point ($\mathbf{Q} = 0$, as in optical measurements) but also at $\mathbf{Q} \neq 0$. In fact, at $\mathbf{Q} = 0$ the effective dielectric function is dominated by the underlying substrate [16], and the surface states do not contribute to the EELS spectrum. At $\mathbf{Q} \neq 0$ the surface excitons have higher excitation energy, showing an upwards dispersion with an effective mass of about $1.1m_e$ in our calculations. Because of this dispersion and due to the increasing surface sensitivity at $\mathbf{Q} \neq 0$, the largest part of EELS intensity results from surface excitons with energies above 9.3 eV. Our resulting EELS spectrum is in nice agreement with the measured data,

apart from the remaining energy difference of about 0.6 eV for the surface-exciton peak. This might be related to the slight underestimation of the ionization potential by our results.

In experimental EELS data of MgO(001) the surface peak is observed at about 6.3 eV [1,4]. Assuming that this peak may also be blueshifted by about 0.6 eV relative to the lowest singlet surface exciton (which we find at 5.9 eV), we obtain a peak position of about 6.5 eV in agreement with the measured data.

In conclusion, we have discussed delocalized image states and surface excitations at insulator surfaces with negative electron affinity within *ab initio* many-body perturbation theory (*GW* approximation and Bethe-Salpeter equation). The accurate determination of these states requires inclusion of basis functions in the vacuum and allowance for wave-function mixing in the QP theory. The image states are responsible for low-energy features in the electron energy-loss spectra at 9.9 eV for LiF(001) and 6.5 eV for MgO(001), which is several eV below the bulk excitations.

This work is supported by the Deutsche Forschungsgemeinschaft (Grant No. Ro 1318/4-1 and Ro 1318/5-1).

-
- [1] See, e.g., P.R. Underhill and T.E. Gallon, *Solid State Commun.* **43**, 9 (1982); G. Roy, G. Singh, and T.E. Gallon, *Surf. Sci.* **152/153**, 1042 (1985); T.E. Gallon, *Surf. Sci.* **206**, 365 (1988); P. Wurz *et al.*, *Phys. Rev. B* **43**, 6729 (1991); H. Tatewaki and E. Miyoshi, *Surf. Sci.* **327**, 129 (1995); H. Winter *et al.*, *J. Phys. B* **35**, 3315 (2002).
 - [2] P. A. Cox and A. A. Williams, *Surf. Sci.* **175**, L782 (1986).
 - [3] T. Mabuchi, *J. Phys. Soc. Jpn.* **57**, 241 (1988).
 - [4] M.-C. Wu, C. M. Truong, and D.W. Goodman, *Phys. Rev. B* **46**, 12688 (1992).
 - [5] W. Pong and C. S. Inouye, *J. Electron Spectrosc. Relat. Phenom.* **11**, 165 (1977).
 - [6] See, e.g., M.W. Cole and M.H. Cohen, *Phys. Rev. Lett.* **23**, 1238 (1969).
 - [7] M. Rohlfling and S.G. Louie, *Phys. Rev. B* **62**, 4927 (2000).
 - [8] N.-P. Wang, M. Rohlfling, P. Krüger, and J. Pollmann, *Phys. Rev. B* **67**, 115111 (2003).
 - [9] M. Piacentini, D.W. Lynch, and C. G. Olson, *Phys. Rev. B* **13**, 5530 (1976).
 - [10] R.C. Whited, C.J. Flaten, and W.C. Walker, *Solid State Commun.* **13**, 1903 (1973).
 - [11] M. Rohlfling, *Int. J. Quantum Chem.* **80**, 807 (2000).
 - [12] I. D. White, R.W. Godby, M. M. Rieger, and R. J. Needs, *Phys. Rev. Lett.* **80**, 4265 (1998).
 - [13] O. Pulci, F. Bechstedt, G. Onida, R. Del Sole, and L. Reining, *Phys. Rev. B* **60**, 16758 (1999).
 - [14] The influence of the repeated-slab geometry on Σ has been corrected analytically.
 - [15] A. A. Lucas and J. P. Vigneron, *Solid State Commun.* **49**, 327 (1984).
 - [16] P. Lambin, P. Senet, A. Castieux, and L. Philippe, *J. Phys. I* **3**, 1417 (1993).